HHS Public Access

Author manuscript

J Comp Neurol. Author manuscript; available in PMC 2018 November 01.

Published in final edited form as:

J Comp Neurol. 2017 November 01; 525(16): 3563–3578. doi:10.1002/cne.24291.

Sodium channel subtypes are differentially localized to pre- and post-synaptic sites in rat hippocampus

Kenneth W. Johnson[1], **Karl F. Herold**[1], **Teresa A. Milner**[2,4], **Hugh C. Hemmings Jr.**[1,3], and **Jimcy Platholi**[1,2]

[1]Department of Anesthesiology, Weill Cornell Medicine, New York, NY

[2]Feil Family Brain and Mind Research Institute, Weill Cornell Medicine, New York, NY

[3]Department of Pharmacology, Weill Cornell Medicine, New York, NY

[4]Harold and Milliken Hatch Laboratory of Neuroendocrinology, The Rockefeller University, NY NY

Abstract

Voltage-gated Na^+ channels (Na_v) modulate neuronal excitability, but the roles of the various Na_v subtypes in specific neuronal functions such as synaptic transmission are unclear. We investigated expression of the three major brain Na_v subtypes (Na_v 1.1, Na_v 1.2, Na_v 1.6) in area CA1 and dentate gyrus of rat hippocampus. Using light and electron microscopy, we found labeling for all three Na_v subtypes on dendrites, dendritic spines, and axon terminals, but the proportion of pre- and post-synaptic labeling for each subtype varied within and between subregions of CA1 and dentate gyrus. In the central hilus (CH) of the dentate gyrus, Na_v 1.1 immunoreactivity was selectively expressed in presynaptic profiles, while Na_v 1.2 and Na_v 1.6 were expressed both pre- and post-synaptically. In contrast, in the stratum radiatum (SR) of CA1, Na_v 1.1, Na_v 1.2, and Na_v 1.6 were selectively expressed in postsynaptic profiles. We next compared differences in Na_v subtype expression between CH and SR axon terminals and between CH and SR dendrites and spines. Na_v 1.1 and Na_v 1.2 immunoreactivity was preferentially localized to CH axon terminals compared to SR, and in SR dendrites and spines compared to CH. No differences in Na_v 1.6 immunoreactivity was found between axon terminals of CH and SR or between dendrites and spines of CH and SR. All Na_v subtypes in both CH and SR were preferentially associated with asymmetric synapses rather than symmetric synapses. These findings indicate selective presynaptic and postsynaptic Na_v expression in glutamatergic synapses of CH and SR supporting neurotransmitter release and synaptic plasticity.

Address correspondence to: Dr. Jimcy Platholi, 1300 York Ave, LC-208, Box 50, New York, New York, 10065, P: 212 746 6184, F: 212 746 8316, Jip2003@med.cornell.edu.

Conflict of Interest Statement

The authors declare no conflicts of interest.

Associate Editor: Dr. Deanna Benson

Editor-in-Chief: Dr. Patrick Hof

Role of Authors

All authors had full access to all the data in the study and take responsibility for the integrity of the data and the accuracy of the data analysis. Study concept and design: JP, HCH, TAM. Acquisition of data: JP, KWJ. Analysis and interpretation of data: KFH, KWJ, JP. Drafting of the manuscript: JP. Critical revision of the manuscript for important intellectual content: TAM, HCH, JP. Statistical analysis: KFH. Obtained funding: HCH, TAM. Administrative, technical, and material support: TAM, KWJ. Study supervision: HCH, TAM, JP.

Keywords

Excitatory synapses; RRID:AB_2040003; RRID:AB_2040005; RRID:AB_2040202; RRID:CVCL_6911; RRID:SCR_002798

Introduction

Voltage-gated Na^+ channels (Na_v) contribute to the initiation and propagation of action potentials, and are critical to neuronal excitability (Hodgkin and Huxley, 1952). The distribution and subcellular targeting of Na_v subtypes determine their specific neuronal functions. Presynaptically, Na_v are expressed in the axon initial segment (AIS), nodes of Ranvier, and axon terminals (Boiko et al., 2003; van Wart et al., 2007; Lorincz and Nusser, 2008; Hu et al., 2009). Upon depolarization, Na_v opening generates action potentials at the AIS, transmits action potentials along the axon, and triggers neurotransmitter release at the presynaptic terminal (Colbert and Pan, 2002). Na_v are important drug targets in excitable tissues, and are principal targets of anti-epileptics, local anesthetics, and general anesthetics, drugs that reduce electrical activity and synaptic transmission (Errington et al., 2008; Mantegazza et al., 2010; Herold and Hemmings, 2012; Catterall, 2014).

Dendritic Na_v modulate synaptic strength and intrinsic excitability, and are involved in synaptic plasticity (Magee and Johnston, 1997; Svoboda et al., 1999; Larkum and Zhu, 2002; Sjöstrom and Nelson, 2002; Dan and Poo, 2004; Xu et al., 2005). For example, Na_v-mediated depolarization allows Ca^{2+} influx through NMDA-type glutamate receptors (NMDAR) and L-type voltage-gated Ca^+ channels (Cav) essential for long-term potentiation (LTP; Golding et al., 2002; Kim et al., 2015). Pharmacological inhibition of Na_v reduces activity-dependent recruitment of neurotrophins necessary for learning and memory and attenuates LTP in hippocampal pyramidal neurons (Dean et al., 2012; Kim et al., 2015).

Action potentials initiated by Na_v in axons can forward–propagate to activate exocytosis, while back-propagated or locally generated action potentials in apical dendrites and spines play a critical role in synaptic plasticity (Magee and Johnston, 1997; Stuart et al., 1997; Buzsaki and Kandel, 1998; Tsay and Yuste, 2002). Axonal and somatodendritic Na^+ currents vary in their gating properties, suggesting that different Na_v subtypes and/or auxiliary subunits are preferentially localized and contribute to distinct Na_v-dependent physiological functions (Colbert et al., 1997; Gasparini and Magee, 2002).

Three major Na_v subtypes (Na_v 1.1, Na_v 1.2, Na_v 1.6) are expressed in adult mammalian brain, each consisting of a specific α-subunit and one or more auxiliary β-subunits (Catterall, 1984; Yu and Catterall, 2003). Immunolabeling for all three subtypes has been detected by light microscopy in presynaptic compartments in various brain regions (Caldwell et al, 2000; Boiko et al., 2003; van Wart et al., 2007; Lorincz and Nusser, 2008; Hu et al., 2009), while Na_v 1.1 and Na_v 1.2 are selectively expressed in the soma (Westenbroek et al., 1989; Gong et al., 1999). In the hippocampus, Na_v 1.6 and Na_v 1.2 have greater dendritic expression in area CA1 (Lorincz and Nusser, 2010), while Na_v 1.1 labeling is concentrated in the AIS and nodes of Ranvier in the dentate gyrus (DG; Ogiwara et al.,

2007; Duflocq et al., 2008). Comprehensive analysis of differences in the subcellular expression of the major brain Na_v subtypes are unknown.

The hippocampus consists of subregions with distinct cell populations and architecture. The majority of hippocampal neurons are excitatory principal cells that form asymmetrical synapses (van Groen and Wyss, 1990; Blasco-Ibanez and Freund, 1995). In contrast, inhibitory neurons are fewer in number and form symmetric synapses (Freund and Buzsaki, 1996). We hypothesized that Na_v subtype expression is heterogeneous between different hippocampal subregions. Area CA1 and DG are two well-characterized subregions with distinct cell populations, subcellular structures, and functions. Area CA1 is primarily an excitatory region receiving glutamatergic input from area CA3 and entorhinal cortex (Amaral and Witter, 1989; Megias et al., 2001). LTP in the CA1 region is an extensively studied model of activity-dependent plasticity in the mammalian brain (Malenka and Nicoll, 1993; Malenka, 2003). The stratum radiatum (SR) is a representative subfield of CA1 containing mostly pyramidal neurons with few basket cell interneurons (Freund and Buzsaki, 1996). Similarly, the DG receives excitatory projections from the entorhinal cortex, but one of its sublayers, the central hilus (CH), also contains multiple interneurons including basket cells, chandelier cells, and dendritic inhibitory cells (Freund and Buzsaki, 1996; Amaral et al., 2007). Intracellular labeling and post-embedding immunogold staining for GABA confirm these interneurons as mostly GABAergic (Kosaka et al., 1985, 1988; Soriano and Frotscher, 1989; Halasy and Somogyi, 1993).

We used both light and electron microscopic immunocytochemistry to determine the spatial distributions of Na_v 1.1, Na_v 1.2, and Na_v 1.6 in rat hippocampal subfields SR (CA1) and CH (DG). To gain functional insights, we separately analyzed and quantified the expression of all three Na_v subtypes in pre- and post-synaptic structures identified by electron microscopy.

Materials and Methods

Animals and tissue preparation

Procedures for animal treatment and tissue collection were approved by the Institutional Animal Care and Use Committee (IACUC) of Weill Cornell Medicine and were in strict accordance with the recommendations in the Guide for the Care and Use of Laboratory Animals of the National Institutes of Health. Three adult male Sprague-Dawley rats (2 months old, 220-250 g; Charles River Laboratories, Wilmington, MA) were used for immunocytochemical studies. Rats were deeply anesthetized with sodium pentobarbital (150 mg/kg, i.p.) and transcardially perfused sequentially with: 1) 15 ml 0.9% (w/v) NaCl containing 1,000 units/ml heparin; 2) 50 ml 3.75% (w/v) acrolein and 2% (w/v) paraformaldehyde in 0.1M phosphate buffer (PB; pH 7.4), and 3) 200 ml of 2% (w/v) paraformaldehyde in PB (Milner et al., 2011). Each brain was removed, cut into 5 mm coronal blocks using a brain mold (Activational Systems, Warren, WI) and post-fixed in 2% (w/v) paraformaldehyde in PB for 30 min. Following post-fixation, regions containing the hippocampal formation (HF) were cut into 40 μm thick coronal sections using a vibrating microtome (Vibratome, Leica Biosystems, Buffalo Grove, IL) and collected into PB.

Sections were stored at −20°C in cryoprotectant (30% sucrose, 30% ethylene glycol in PB) until immunocytochemical processing (Milner et al., 2011).

Cell culture and transfection

Rat hippocampal cells were cultured according to Calabrese & Halpain (2005). Briefly, whole hippocampi were dissected from embryonic day 18 Sprague Dawley rats, and the cells dissociated, cultured on glass coverslips (Carolina Biological, Burlington, NC) in 24-well plates (BD Biosciences, San Jose, CA) at a density of 300 cells/mm^2, and maintained in Neurobasal medium (GIBCO, Grand Island, NY) supplemented with SM1 (Stem Cell Technologies, Vancouver, Canada) and 0.5 mM L-glutamine (Sigma-Aldrich, St. Louis, MO). For some experiments, the hippocampus was separated into CA and DG regions prior to dissociation. Neurons were transfected at 21 days *in vitro* (DIV) using calcium phosphate precipitation with 4–6 μg pEGFP-N1 (Clontech, Mountain View, CA) according to Kohrmann et al. (1999) to allow visualization of dendritic and axonal morphology by fluorescence microscopy. Cells were incubated with the transfection mixture for 2.5 h in 95% air/5% CO_2 at 37°C, washed twice with pre-warmed HBS (in mM: 135 NaCl, 4 KCl, 1 Na_2HPO_2, 2 $CaCl_2$, 1 $MgCl_2$, 10 glucose, and 20 HEPES [pH 7.35]), and replaced with Neurobasal medium.

The HEK293FT (RRID:CVCL_6911) human embryonic kidney cell line (Invitrogen, Carlsbad, CA) was used for antibody verification as they do not express endogenous Na_v 1.1, Na_v 1.2 or Na_v 1.6 (He and Soderlund, 2010). Cells were cultured in Dulbecco's modified Eagle's medium (Invitrogen, Carlsbad, CA) supplemented with 10% (v/v) fetal bovine serum (Invitrogen), 2 mM L-glutamine, 100 U/ml penicillin, and 100 μg/ml streptomycin (Invitrogen) and 50 mg/ml Geneticin (Thermo Scientific, Rockford, IL) at 37°C under 95% air/5% CO_2. Cells were grown on 12-mm glass coverslips in 35-mm polystyrene culture dishes and transiently transfected with human Na_v 1.1 (pCMV vector), rat Na_v 1.2 (pcDM8 vector), or mouse Na_v 1.6 (modified pcDNA vector) with pEGFP-N1 (Clontech, Mountain View, CA) as a reporter plasmid (0.5–1 μg), or reporter plasmid alone, using Lipofectamine LTX (Invitrogen). The Na_v clones were kindly provided by: Alfred L. George Jr. (Northwestern University, Chicago, IL)-human Na_v 1.1; William Catterall (University of Washington, Seattle, WA)-rat Na_v 1.2a; Stephen Waxman (Yale University, New Haven, CT)-mouse Na_v 1.6. At 48 h after transfection, the transfected cells were fixed and identified by expression of eGFP using fluorescence microscopy.

Antibodies

Antibodies to Na_v 1.1 (Alomone Labs Cat# ASC-001 Lot# RRID:AB_2040003), Na_v 1.2 (Alomone Labs Cat# ASC-002 Lot# RRID:AB_2040005), and Na_v 1.6 (Alomone Labs Cat# ASC-009 Lot# RRID:AB_2040202) were purchased from Alomone (Jerusalem, Israel). All antibodies were affinity-purified rabbit polyclonal antisera raised against synthetic peptides corresponding to the intracellular loop between domains I and II of rat Na_v 1.1 and Na_v 1.2, and between domains II and III of rat Na_v 1.6 (Table 1). Validation of all three Na_v antibodies from Alomone has been demonstrated (Alomone; Cheng et al., 2014; Blanchard et al., 2015; Cesca et al., 2015; Liu et al., 2015). Antibody specificity was confirmed using

immunoblotting and immunocytochemistry of primary neurons and HEK cells as described below.

Hippocampal primary cell lysates or lysates from untransfected and transfected HEK293FT cells were harvested and solubilized in lysis buffer (50 mM Tris-HCl; pH 7.5, 150 mM NaCl, 1% NP-40, 0.25% sodium deoxycholate, 1 mM EDTA, and protease inhibitors) at 4°C for 30 min and centrifuged at 100,000 *g* for 30 min to remove insoluble material. For immunoprecipitation, rat hippocampal lysate (0.5 ml of 1.5 μg/ml protein) was prepared (Tippens and Lee, 2007) and incubated with Na_v antibodies (5 μg) for 1 h rotating at 4°C. Protein concentrations were determined by BCA protein assay kit (Thermo Scientific) using bovine serum albumin (BSA) as standard. Protein-A-Sepharose (RepliGen, Waltham, MA; 50 μl of 50% slurry) was added and reactions continued for an additional 2 h rotating at 4°C. Following three washes in lysis buffer, proteins were eluted with sodium dodecyl sulfate (SDS)-containing sample buffer and subjected to SDS-polyacrylamide gel electrophoresis (PAGE). Proteins from transfected cells or immunoprecipitated from brain or cell lysates were detected by immunoblotting (Pierce Fast Western Blot Kit, Thermo Scientific) after transfer to polyvinylidine difluoride membranes (0.45 μm, BioRad, Hercules, CA) as described (Hemmings et al., 1992). Membranes were incubated in blocking buffer (5% dried milk powder (w/v) in PBST [10 mM Na-phosphate, 250 mM NaCl, 0.5% (v/v) Tween 20, pH 7.8]) for 1 h, and then with anti-Na_v 1.1 (1:400), Na_v 1.2 (1:200), or Na_v 1.6 (1:800) without or with an equal concentration of preadsorption control peptide antigen for 1 h. Membranes were washed three times for 10 min with PBST, and bound antibody was detected using horseradish-peroxidase (HRP)-conjugated anti-rabbit antibodies (1:10) with enhanced chemiluminescent detection reagents (Thermo Scientific).

Immunocytochemistry

Primary hippocampal neurons or HEK293FT cells were fixed with 3.7% (w/v) formaldehyde in phosphate-buffered saline (150 mM NaCl, 2.7 mM KCl, 10 mM Na2HPO4, 2 mM KH2PO4, pH 7.4; PBS) plus 120 mM sucrose for 20 min at 37°C. Fixed cells were rinsed with PBS and permeabilized with 0.2% (w/v) Triton X-100 in PBS for 4 min at room temperature, then blocked for 30 min with 2% (w/v) BSA in PBS. Antibodies to the following antigens were used: guinea pig polyclonal vGlut1 (Synaptic Systems, Goettingen, Germany) at 1:10,000, mouse monoclonal GAD2/GAD65 (Synaptic Systems) at 1:1000, and rabbit polyclonal Na_v 1.1 (1:400), Na_v 1.2 (1:200) and Na_v 1.6 (1:800) (Alomone). Antibodies were incubated with fixed cells for 1 h at room temperature. Following rinsing with PBS, fixed cells were incubated with AlexaFluor-488 or AlexaFluor-568-conjugated secondary antibody (Invitrogen/Molecular Probes, Eugene, OR) for 45 min at 37°C and washed three times for 10 min. Coverslips were mounted and fluorescence images were collected using a CSU-X1 spinning disk confocal (Yokogawa, Japan) mounted onto a Zeiss Z1 Observer and a 63× 1.4 (NA) Plan APO oil immersion or 20× 0.8 (NA) Plan APO air objective. Cells were excited using 50 mW solid state lasers (488 and 561 nm) with 525/50 and 629/62 band-pass filters. A series of images was acquired in the z dimension at optical slice thickness of 0.2 to 0.4 μm using an ORCA-Flash 4.0 camera (Hamamatsu, Japan) with Zeiss Zen software. Acquired fluorescence images were adjusted for brightness and contrast in ImageJ 1.49 (NIH, Bethesda, MD).

Immunoperoxidase labeling

Free-floating sections from fixed rat dorsal hippocampus were processed together to minimize differences in immunocytochemical labeling (Pierce et al., 1999; Spencer et al., 2008). Sections were processed for immunocytochemical localization using an avidinbiotin complex (ABC) protocol (Hsu et al., 1981) as modified by Milner et al., (2011). Briefly, hippocampal sections were washed 1) 3 times 10 min in PB to remove cryoprotectant; 2) 30 min in 1% sodium borohydride in PB to remove active aldehydes; and 3) in PB to remove sodium borohydride. All sections were then incubated in: 1) 0.5% BSA in Tris-saline solution (TS; 0.9% NaCl in 0.1 M Tris HCl, pH 7.6) to block non-specific binding; 2) primary antibody in 0.1% BSA in TS (Na_v 1.1 1:3000, Na_v 1.2 1:2000, Na_v 1.6 1:2000) for 1 day at room temperature, followed by 3-4 days at 4°C; 3) donkey anti-rabbit biotinylated IgG 1:400 for 30 min; 4) peroxidase-avidin complex 1:100 (Vectastain Elite Kit) for 30 min; and 5) 3,3′-diaminobenzidine (DAB; Sigma Aldrich, Milwaukee, WI) and H2O2 in TS for 6-8 min. All incubations were separated by three washes in TS.

For light microscopy, sections were rinsed in PB and mounted onto gelatin-coated glass slides. Sections were dehydrated and coverslipped with DPX mounting medium (Sigma Aldrich).

For electron microscopy, sections were postfixed for 1 h in 2% (w/v) osmium tetroxide in PB, dehydrated through an increasing series of ethanol and propylene oxide, and embedded in EMBed 812 (EMS, Hatfield, PA) for 12 h, mounted between two sheets of plastic and incubated at 60°C for 3 days (Milner et al., 2011). Sections from the midseptotemporal level of the dorsal hippocampus [between AP −3.25 and −4.20 from bregma (Swanson, 2003)] were selected, mounted on EMBed chucks and trimmed to 1-1.4 mm trapezoids. Ultrathin sections (70 nm thick) close to the plastic-tissue interface (within 0.1-0.2 μm) were cut on a Leica UTC ultramicrotome, collected on 400-mesh thin bar grids (EMS, Fort Washington, PA), and counterstained with uranyl acetate (20 min) and Reynold's lead citrate (1 min). Final preparations were analyzed on a CM10 transmission electron microscope (FEI, Hillsboro, OR), and images were acquired with a digital camera system (Advanced Microscopy Techniques, v. 3.2). For figures, digital images were adjusted for level, brightness, contrast, and sharpness in ImageJ 1.49. Final graphs were assembled using Prism 7.0 (https://www.graphpad.com/scientific-software/prism/, RRID:SCR_002798).

Quantitative analysis

Electron microscopic examination of immunoreactivity was performed on hippocampal sections from three rats. From each section, stratum oriens (SO), stratum radiatum (SR) and stratum lacunosum-moleculare (SLM) of CA1 and molecular cell layer (MCL) and central hilus (CH) of DG were imaged. Quantitative analysis of Na_v 1.1, Na_v 1.2 and Na_v 1.6 immunoreactivity was performed on SR and CH. Five random, non-overlapping micrographs (70 μm^2/micrograph) per lamina per brain region were examined. Immunolabeled profiles were classified according to Peters et al. (1991): Dendrites were defined by the presence of microtubules, neurofilaments, and occasional mitochondria and were often postsynaptic to axon terminals. Dendritic spines sometimes contained a spine apparatus, were mostly devoid of mitochondria, and often contacted by axon terminals.

Unmyelinated axons were < 0.2 μm in diameter, contained microtubules and occasional synaptic vesicles, and lacked synaptic junctions in the plane of the section. Axon terminals had a cross-sectional diameter ˃ 0.2 μm, contained clear synaptic vesicles and occasional dense core vesicles, and often showed a junctional synaptic specialization. Asymmetric synapses (potentially excitatory) contained a prominent postsynaptic density, intercleft material and possessed a widened synaptic. Symmetric synapses (potentially inhibitory) had a less pronounced postsynaptic density, less intercleft material and a narrower synaptic cleft compared to asymmetric synapses.

Data quantification and analysis were performed by investigators (JP, KFH) blinded to the experimental condition. First, all synapses (labeled and unlabeled) were identified from 5 micrographs (70 μm^2) for 3 sets totaling 1050 μm^2 of tissue examined for each lamina. Second, Na_v immunoreactivity in labeled synapses was pooled by profile type (presynaptic-axon terminals; postsynaptic-dendrites, spines). Five micrographs (total area 350 μm^2 for one experiment) were analyzed for each antibody, and pre- and post-synaptic profiles were compared *within* the SR and CH laminae using unpaired two-tailed t-tests to determine: pre- or post-synaptic preference for specific Na_v subtype expression in CH synapses; and pre- or post-synaptic preference for specific Na_v subtype expression in SR synapses. The same pre- and post-synaptic profiles were compared *between* layers using unpaired two-tailed t-tests to determine: differences in specific Na_v subtypes expressed between axon terminals in CH and SR; and differences in specific Na_v subtypes expressed between dendrites and spines in CH and SR. Data for each profile type are described as percentage of total synapses per group. We further classified *labeled* synapses as symmetric or asymmetric for each Na_v subtype and layer as follows: Pre- or postsynaptic profiles containing Na_v labeling were identified. From these *labeled* profiles, the percentage forming symmetric or asymmetric synapses were determined and compared using two-tailed *t* tests, followed by correction for multiple comparisons by the Holm-Sidak method (N=3). Data are expressed as percentage of labeled synapses from total synapses in each lamina or as percentage of total labeled synapses. Significance was set at $p<0.05$ and data are expressed as mean ± SEM. Data analysis was performed using GraphPad Prism 7.0 and Excel (Microsoft, Redmond, Washington).

Results

Validation of Na_v antibodies

Antibodies to the three major Na_v subtypes expressed in rat brain (Na_v 1.1, Na_v 1.2, and Na_v 1.6) were used to examine their ultrastructural localization in rat hippocampal subfields. Antibodies were affinity-purified antisera with specificity confirmed as follows: Antibodies immunoprecipitated proteins corresponding in molecular mass to Na_v 1.1 (~260 kDa) or Na_v 1.2 (~280 kDa) from rat hippocampal brain lysates (Fig. 1A, B). Immunoblotting of hippocampal lysates with anti-Na_v 1.1 confirmed expression of Na_v 1.1, which was not detected by anti-Na_v 1.2 or anti-Na_v 1.6 (Fig. 1A). Similar specificity was verified for anti-Na_v 1.2 (Fig. 1B). We were unable to immunoprecipitate Na_v 1.6 from rat hippocampal lysates although at least one study has shown immunoblotting of Na_v 1.6 with the same antibody after immunoprecipitation with amyloid precursor protein from mouse brain (Liu et al., 2015). Concentration of Na_v 1.6 (whole brain *vs* hippocampus) and temperature used to

denature samples (35°C *vs.* 95°C) could have affected sample amount or degradation. To circumvent this, lysates from HEK293FT cells transfected with cDNA corresponding to Na_v 1.1, Na_v 1.2 or Na_v 1.6 were used (Blanchard et al., 2015). Transfection was verified by measuring Na^+ currents using patch-clamp electrophysiology (data not shown), and immunoblotting with anti-Na_v 1.6 confirmed expression, molecular mass (~245 kDa) and specificity of anti-Na_v 1.6 (Fig. 1C) with a preadsorption antigen peptide used as a control (Fig. 1C, right two lanes). In addition, specificity for Na_v 1.6 was confirmed by specific immunofluorescence labeling using anti-Na_v 1.6 of HEK293FT cells transfected with eGFP and Na_v 1.1, Na_v 1.2 or Na_v 1.6 (Fig. 1D; Supp. Fig. 1D for red/green). Co-transfection efficiency was less than 100%, but all cells expressing Na_v 1.6 also expressed eGFP (Fig. 1D, arrows; Supp. Fig. 1D for red/green).

Light microscopic localization of Na_v immunoreactivity

Strong immunoreactivity for Na_v 1.1, Na_v 1.2, and Na_v 1.6 was detected in the pyramidal cell layer (PCL) of the hippocampus proper (Fig 2B, top panels) and the granule cell layer (GCL) of the DG (Fig. 2C, top panels) using DAB detection by light microscopy. In CA1, immunoreactivity for all three Na_v subtypes extended from the pyramidal cell soma into the basal dendrites of the stratum oriens (SO) and into apical dendrites of the stratum radiatum (SR) and stratum lacunosum moleculare (SLM) (Fig 2B, top panels). Similarly, surrounding laminae of granule cells of the DG showed Na_v immunoreactivity continuing into the molecular layer (ML) as well as into the central hilus (CH) (Fig 2C, top panels).

Immunofluorescence labeling for all Na_v subtypes was also observed in primary rat hippocampal neurons isolated from CA1 (Fig 2B, bottom panels; Supp. Fig. 2B for red/green) and DG (Fig 2C, bottom panels; Supp. Fig. 2B for red/green). Na_v is expressed in both excitatory and inhibitory neurons (Westenbroek et al., 1989; Trimmer and Rhodes, 2004), with cell type-dependent differences in subtype expression accounting for variability in action potential initiation site and firing properties (Ogiwara et al., 2007; Lorincz and Nusser, 2008). To determine whether excitatory and inhibitory presynaptic terminals differ in Na_v subtype expression, hippocampal cultures were co-labeled with Na_v and axon terminal markers selective for excitatory (vGlut-glutamate) or inhibitory (GAD65-GABA) neurotransmitters. We observed partial co-localization for vGlut or GAD65 in all Na_v subtypes (Fig 2D, Na_v 1.1 shown; Supp. Fig. 2D for red/green).

Electron microscopic immunolocalization of Na_v 1.1, Na_v 1.2, and Na_v 1.6

At the electron microscopic level, Na_v 1.1, Na_v 1.2, and Na_v 1.6 labeling was found in all laminae of the CA1 and DG examined. Labeling by all three Na_v antibodies was found in dendrites, dendritic spines, axon terminals (Figs. 3–5), and glia (data not shown). Peroxidase reaction product was seen as discrete spots in dendritic shafts (Fig. 3), dendritic spine heads (Fig. 4), and in axons and axon terminals (Fig. 5) for all three antibodies. Na_v labeling in dendritic shafts was found in patches (Fig. 3) and sometimes on endomembranes near mitochondria (Fig. 3C, 3E), while dendritic spine labeling in all laminae was found mainly on spine heads (Fig. 4). Quantitative analysis focused on CA1 stratum radiatum (SR) and DG central hilus (CH) since these subregions have distinct neuroanatomical organizations

with layer-specific differences in excitatory and inhibitory inputs that allow correlation with neuronal phenotype.

Na_v 1.1 is predominantly presynaptic in central hilus while all three subtypes are largely postsynaptic in stratum radiatum

Labeled and unlabeled synapses were identified in the stratum radiatum (SR) and central hilus (CH; Fig 6A) with a total area of 1050 μm^2 tissue examined for each antibody per subregion. Expression of Na_v in axon terminals was considered presynaptic, while expression in dendrites or dendritic spines was considered postsynaptic. Analysis was conducted as follows: 1) All synapses (labeled and unlabeled) were counted in the total area, 2) From these synapses, Na_v labeling was quantified in the presynaptic compartments as a percentage of the total number synapses, 3) Na_v labeling was quantified in the postsynaptic compartments as a percentage of the total number of synapses (Fig 6A,C). Percentages serve as a relative comparison between Na_v labeling in pre- and post-synaptic compartments, and so do not add up to 100% as not all synapses are labeled (Fig 6A,B) and some synapses have both pre- and post-synaptic Na_v labeling (Fig 6A,C). Using this method, we found that Na_v 1.1 immunoreactivity was more frequently localized to axon terminals compared to dendrites and spines (61% *vs.* 30%; Fig 6D, left) in CH, whereas SR showed more Na_v 1.1 labeling in dendrites and spines than in axon terminals (29% *vs.* 49%; Fig. 6D, right). These SR postsynaptic compartments also had significantly more Na_v 1.2 (17% *vs.* 48%) and Na_v 1.6 (18% *vs.* 45%) labeling (Fig. 6D, right), while no differences in distribution for Na_v 1.2 (41% *vs.* 39%) or Na_v 1.6 (32% *vs.* 43%) were found in CH (Fig. 6D, left). Unlabeled synapses were similarly distributed in CH and SR (30-50%; Fig 6B).

Na_v 1.1 and Na_v 1.2 are highly expressed in axon terminals in central hilus compared to stratum radiatum and in dendrites and spines in stratum radiatum compared to central hilus

Na_v are closely coupled to neurotransmitter release at axon terminals (Lai and Jan, 2006). Along with Cav and K^+ channels, Na_v regulate presynaptic Ca^{2+} entry into the terminal critical for neurotransmitter release (Dittman and Ryan, 2009). Specific Na_v subtypes involved in exocytosis of particular transmitters or in specific synapses are essentially unknown. To identify subregional differences related to presynaptic Na_v function based on subtype expression, we compared presynaptic Na_v immunoreactivity between CH and SR (Fig. 6E) using the same profiles. Axon terminals in CH exhibited greater Na_v 1.1 and Na_v 1.2 immunoreactivity compared to axon terminals in SR (Na_v 1.1: 61% *vs.* 28%; Na_v 1.2: 41% *vs.* 17%; Fig. 6E, left). In contrast, Na_v 1.1 and Na_v 1.2 showed more labeling on dendrites and spines in SR compared to dendrites and spines in CH (Na_v 1.1: 49% *vs.* 29%; Na_v 1.2: 48% *vs.* 39%; Fig. 6E, right). Such differential regional and subcellular expression of specific Na_v subtypes suggests distinct regulatory roles in modulating network excitability and exocytosis. No significant differences were found for Na_v 1.6 expression in axon terminals, dendrites, or spines between CH (32% *vs.* 18%) and SR (43% *vs.* 45%) (Fig. 6E).

All Na_v subtypes are primarily expressed at asymmetric synapses

Na_v can play different roles based on cellular and subcellular localization, and our results show regional differences in Na_v subtype expression between pre- and post-synaptic sites.

To determine whether inhibitory and excitatory presynaptic terminals differ in expression of Na_v subtypes, we examined Na_v subtype immunoreactivity in pre- and postsynaptic structures from SR and CH by identifying terminals forming or dendrites receiving symmetric or asymmetric synapses, which are likey inhibitory or excitatory, respectively (Fig. 7A; Peters et al., 1991).

Pre- or post-synaptic profiles containing Na_v labeling were identified. From these *labeled* profiles, the percentage forming symmetric or asymmetric synapses were determined. We observed distinct patterns of Na_v expression in SR with preferred labeling for all subtypes in postsynaptic compartments (Fig. 7B). Immunolabeling mostly occurred on dendritic spines, and was mainly associated with asymmetric synapses (Fig. 7B). In CH, greater expression of Na_v 1.1 was found on presynaptic terminals (Fig. 6D,E, left panels), but all Na_v subytpes were also mainly associated with asymmetric synapses (Fig 7C).

Discussion

The major brain Na_v subtypes exhibit distinct patterns of cellular and subcellular expression in rat hippocampus. Na_v 1.1, Na_v 1.2, and Na_v 1.6 were expressed in dendrites, dendritic spines, and axon terminals, with differences between stratum radiatum (SR) and central hilus (CH). All three Na_v subtypes are expressed in dendritic spines in all layers of CA1 and DG. In CH, Na_v 1.1 immunoreactivity was predominantly presynaptic, with no significant differences in pre- or post-synaptic expression for Na_v 1.2 or Na_v 1.6 (Fig. 6D, left). In SR, immunoreactivity for all three Na_v subtypes were largely postsynaptic (Fig. 6D, right). Further analysis of Na_v expression between presynaptic and postsynaptic compartments of CH and SR revealed that both Na_v 1.1 and Na_v 1.2 are expressed more in CH axon terminals compared to SR, and in SR dendrites and spines compared to CH (Fig. Fig. 6E). Although a trend for higher expression in CH axon terminal was found, no significant differences in Na_v 1.6 expression in axon terminals or dendrites and spines between CH and SR were found (Fig. 6E). Most pre- and post-synaptic labeling of Na_v in both subregions was associated with asymmetric synapses. Regional and cellular differences in Na_v subtype expression could influence neuronal network interactions for regulating hippocampus-dependent functions through effects on neuronal excitability and synaptic transmission.

Methodological considerations

The antibodies to Na_v 1.1, Na_v 1.2, and Na_v 1.6 used are well characterized having undergone rigorous biochemical and immunocytochemical analyses. They have been used previously in rodent brain, supporting specificity of labeling in rat hippocampus (Cheng et al., 2013; Cesca et al., 2015). Using rat lysates, we confirmed specific labeling for Na_v 1.1 and Na_v 1.2, and of Na_v 1.6 using transfected HEK293FT cells (see also Blanchard et al., 2014).

Labeling by antibodies generated against intracellular sequences can be affected by epitope masking, and Na_v have been shown to interact directly with various auxiliary subunits and protein modulators (Sampo et al., 2000). Incomplete antigen representation would reduce detection and lead to underestimated expression of Na_v in CA1 and DG, particularly in small, less abundant profiles. Analysis of a large number of labeled profiles (1050 μm^2 of

tissue per antibody in three rats) was used to minimize these limitations. In addition, quantitative analysis was conducted between or within regions for the same antibody allowing direct comparisons of similarly processed tissue.

Functional correlations of Na_v expression

A variety of medical conditions are associated with mutations in Na_v subtypes, for example, impaired cognitive performance is associated with reduced Na_v 1.1 expression in mice and humans with a SCN1A mutation (Jensen et al., 2014). Na_v 1.1 mutations also play a role in pain signaling and are associated with hemiplegic migraines (Cestele et al., 2013). Na_v 1.2 mutations are involved in autism (Sanders et al., 2012; Schmunk and Gargus, 2013; Tavassoli et al., 2014), and both Na_v 1.2 and Na_v 1.6 are implicated in the pathophysiology of multiple sclerosis (Waxman, 2008).

Specificity of Na_v function can be determined by subtype-specific gating properties (activation/inactivation), developmental and region-specific expression, and/or targeting to specific subcellular and functional domains of a neuron. For example, Na_v 1.2 is the only subtype expressed at nodes of Ranvier and AIS early in development (Boiko et al., 2003; Osorio et al., 2005), but is replaced by Na_v 1.6 later in development (Tian et al., 2014). Consequently, in mature neurons, action potential generation transitions from Na_v 1.2 to Na_v 1.6, which has a lower voltage threshold for activation and affects seizure susceptibility (Liao et al., 2010; Gazina et al., 2015).

Previous studies have demonstrated Na_v 1.1, Na_v 1.2, and Na_v 1.6 expression in axons and terminals (Duflocq et al., 2008; Lorincz and Nusser, 2008) and Na_v 1.1 and Na_v 1.6 expression in dendrites and spines (Westenbroek et al., 1989; Lorincz and Nusser, 2010) of the hippocampus. We extended these findings using electron microscopy to show that all three major neuronal Na_v subtypes are expressed both pre-and post-synaptically throughout all layers of the hippocampal formation. Quantitative analysis showed Na_v 1.1 and Na_v 1.2 to be predominantly expressed in axon terminals in CH and in dendrites and dendritic spines in SR. This differential expression and localization of channel subtypes within individual neurons suggests that targeting to different neuronal domains can influence both axonal conduction and synaptic function. In axon terminals, Na_v are closely coupled to neurotransmitter release (Lai and Jan, 2006). Functionally distinct dendritic Na^+ currents would allow tuning of presynaptic excitation and postsynaptic responses necessary for specific forms of synaptic plasticity (Stuart et al., 1997). Based on the expression pattern, Na_v 1.1 and Na_v 1.2 are important to neurotransmitter release in CH and action potential backpropagation and synaptic plasticity in SR, interpretations that require neurophysiological confirmation.

Postsynaptic Na_v immunoreactivity in SR was largely in dendritic spines, primary sites of excitatory input. This is in contrast to an earlier electron microscopy study showing somatodendritic, but not dendritic spine localization of Na_v 1.6 in SR (Lorincz and Nusser, 2010), which might be due to differences in antibody and tissue preparation. Moreover, the location of sampling might also have an effect as the amplitude of dendritic Na^+ action potentials steeply decreases with distance from the soma (Svoboda et al., 1999). Many studies support the presence of Na_v in dendritic spines. Densities of Na_v in dendritic shafts

do not account for the effective backpropagation observed, and simulation studies suggest Na_v clustering in spines (Tsay and Yuste et al., 2002; Tønnesen and Nägerl, 2016). Electrical isolation of spines is also supported by Ca^+ imaging, two-photon glutamate uncaging and electrophysiology studies (Araya et al., 2006; Grunditz et al., 2008; Harnett et al., 2012).

Electrophysiological studies show that axonal and dendritic Na^+ currents differ in their activation and inactivation properties (Gasparini et al., 2002), consistent with distinct Na_v subtype compositions. For example, axonal Na^+ currents rapidly activate and completely inactivate compared to sustained somatodendritic Na^+ currents (Westenbroek et al., 1989). We identified specfic Na_v subtypes favoring an axonal or dendritic distribution that can be combined with future electrophysiological studies to delineate distinct neurophysiological functions.

Na_v 1.1 in stratum radiatum and central hilus associates more with asymmetric synapses

Inhibition of Na_v activity has little effect on GABAergic axons (He et al., 2002; Meeks and Mennerick, 2004) suggesting not only region-specific but also transmitter-specific roles of Na_v subtypes. For example, Na^+ currents in interneurons are sustained, less sensitive to inactivation and generally greater than in glutamatergic pyramidal cells (Mickus et al., 1999; Martina et al., 2000). The balance between excitatory and inhibitory transmission is critical for normal neuronal function, and aberrant Na_v activity is central to the pathophysiology of seizures. The DG modulates major excitatory input associated with epileptic activity. Onset of seizures coincides with functional and structural deficits in DG granule cells including a greater reduction of Na_v 1.1-expressing GABAergic neurons and heightened spontaneous excitatory transmission (Tsai et al., 2015). This loss of inhibitory regulation was also found in interneurons but not pyramidal neurons of Na_v $1.1^{+/-}$ mice (Yu et al. 2006; Ogiwara et al., 2007). Thus, transmitter-specific roles of Na_v subtypes are critical to understanding neuronal activation leading to hyperexcitability.

Studies have shown Na_v 1.1 expression only in axonal initial segment of GABAergic interneurons (Ogiwara et al., 2007; Lorincz and Nusser, 2008), but synaptic labeling was not examined. To determine if expression of specific Na_v subtype(s) associates more closely with a particular neurotransmitter, we compared Na_v expression in symmetric or asymmetric synapses. All Na_v subtypes in both the SR and CH were associated more with asymmetric/potentially excitatory synapses (Fig. 7). Although the CH contains many interneurons, most Na_v reactivity was within excitatory terminals and spines most likely representing mossy fiber terminals (> 1 μm in diameter; Peters et al., 1991), which suggests that selective inhibition of mossy terminals might be an effective antiepileptic therapy. Future studies identifying Na_v reactivity specifically within interneurons as well as in additional regions of the CA1 and DG will be necessary for more complete understanding.

Conclusions

Neuronal Na_v subtypes are preferentially expressed in dendrites and dendritic spines receiving potentially excitatory glutamatergic synapses in SR. This dendritic Na_v distribution could be critical for synaptic plasticity associated with learning and memory. In contrast, axon terminals forming potentially glutamatergic synapses highly express Na_v

subtypes in CH suggesting an important role in neurotransmitter release. Region- and synapse-specific localizations of Na_v subtypes have important implications for their diverse neurophysiological functions and the actions of Na_v inhibitors.

Supplementary Material

Refer to Web version on PubMed Central for supplementary material.

Acknowledgments

We thank Ms. June Chan of the Neuroanatomy EM Core, Feil Family Brain and Mind Research Institute and Dr. Cheng Zhou of the Department of Anesthesiology, WCM, for technical assistance.

Supported by NIH Grants GM058055-17A1 (HCH), DA08259 (TAM)

Literature Cited

Amaral DG, Scharfman HE, Lavenex P. The dentate gyrus: fundamental neuroanatomical organization (dentate gyrus for dummies). Progress in Brain Research. 2007; 163:3–22. [PubMed: 17765709]

Amaral DG, Witter MP. The three-dimensional organization of the hippocampal formation: a review of anatomical data. Neuroscience. 1989; 31(3):571–591. [PubMed: 2687721]

Araya R, Jiang J, Eisenthal KB, Yuste R. The spine neck filters membrane potentials. Proceedings of the National Academy of Sciences of the United States of America. 2006; 103(47):17961–17966. [PubMed: 17093040]

Blanchard MG, Willemsen MH, Walker JB, Dib-Hajj SD, Waxman SG, Jongmans MC, Kamsteeg EJ. De novo gain-of-function and loss-of-function mutations of SCN8A in patients with intellectual disabilities and epilepsy. Journal of Medical Genetics. 2015; 52(5):330–337. [PubMed: 25725044]

Blasco-Ibáñez JM, Freund TF. Synaptic input of horizontal interneurons in stratum oriens of the hippocampal CA1 subfield: structural basis of feed-back activation. European Journal of Neuroscience. 1995; 7(10):2170–2180. [PubMed: 8542073]

Boiko T, Van Wart A, Caldwell JH, Levinson SR, Trimmer JS. Functional specialization of the axon initial segment by isoform-specific sodium channel targeting. The Journal of Neuroscience. 2003; 23(6):2306–2313. [PubMed: 12657689]

Buzsáki G, Kandel A. Somadendritic backpropagation of action potentials in cortical pyramidal cells of the awake rat. Journal of Neurophysiology. 1998; 79(3):1587–1591. [PubMed: 9497436]

Calabrese B, Halpain S. Essential role for the PKC target MARCKS in maintaining dendritic spine morphology. Neuron. 2005; 48(1):77–90. [PubMed: 16202710]

Caldwell JH, Schaller KL, Lasher RS, Peles E, Levinson SR. Sodium channel Na(v)1.6 is localized at nodes of ranvier, dendrites, and synapses. Proceedings of the National Academy of Sciences of the United States of America. 2000; 97(10):5616–5620. [PubMed: 10779552]

Catterall WA. The molecular basis of neuronal excitability. Science. 1984; 223(4637):653–661. [PubMed: 6320365]

Catterall WA. Sodium channels, inherited epilepsy, and antiepileptic drugs. Annual Review of Pharmacology and Toxicology. 2014; 54:317–338.

Cesca F, Satapathy A, Ferrea E, Nieus T, Benfenati F, Scholz-Starke J. Functional interaction between the Scaffold Protein Kidins220/ARMS and neuronal voltage-gated Na+ channels. The Journal of Biological Chemistry. 2015; 290(29):18045–18055. [PubMed: 26037926]

Cestèle S, Labate A, Rusconi R, Tarantino P, Mumoli L, Franceschetti S, Gambardella A. Divergent effects of the T1174S SCN1A mutation associated with seizures and hemiplegic migraine. Epilepsia. 2013; 54(5):927–935. [PubMed: 23398611]

Cheng KI, Wang HC, Chuang YT, Chou CW, Tu HP, Yu YC, Lai CS. Persistent mechanical allodynia positively correlates with an increase in activated microglia and increased P-p38 mitogen-activated

protein kinase activation in streptozotocin-induced diabetic rats. European Journal of Pain. 2014; 18(2):162–173. [PubMed: 23868758]

Colbert CM, Magee JC, Hoffman DA, Johnston D. Slow recovery from inactivation of Na+ channels underlies the activity-dependent attenuation of dendritic action potentials in hippocampal CA1 pyramidal neurons. The Journal of Neuroscience. 1997; 17(17):6512–6521. [PubMed: 9254663]

Colbert CM, Pan E. Ion channel properties underlying axonal action potential initiation in pyramidal neurons. Nature Neuroscience. 2002; 5(6):533–538. [PubMed: 11992119]

Dan Y, Poo MM. Spike timing-dependent plasticity of neural circuits. Neuron. 2004; 44(1):23–30. [PubMed: 15450157]

Dean C, Liu H, Staudt T, Stahlberg MA, Vingill S, Bückers J, Chapman ER. Distinct subsets of Syt-IV/BDNF vesicles are sorted to axons versus dendrites and recruited to synapses by activity. The Journal of Neuroscience. 2012; 32(16):5398–5413. [PubMed: 22514304]

Dittman J, Ryan TA. Molecular circuitry of endocytosis at nerve terminals. Annual Review of Cell and Developmental Biology. 2009; 25:133–160.

Duflocq A, Le Bras B, Bullier E, Couraud F, Davenne M. Na_V 1.1 is predominately expressed in nodes of Ranvier and axon initial segments. Molecular and Cellular Neurosciences. 2008; 39(2):180–192. [PubMed: 18621130]

Errington AC, Stöhr T, Heers C, Lees G. The investigational anticonvulsant lacosamide selectively enhances slow inactivation of voltage-gated sodium channels. Molecular Pharmacology. 2008; 73(1):157–169. [PubMed: 17940193]

Freund TF, Buzsáki G. Interneurons of the hippocampus. Hippocampus. 1996; 6(4):347–470. [PubMed: 8915675]

Gasparini S, Magee JC. Phosphorylation-dependent differences in the activation properties of distal and proximal dendritic Na+ channels in rat CA1 hippocampal neurons. Journal of Physiology. 2002; 541(Pt 3):665–672. [PubMed: 12068031]

Gazina EV, Leaw BT, Richards KL, Wimmer VC, Kim TH, Aumann TD, Petrou S. 'Neonatal' Na_V 1.2 reduces neuronal excitability and affects seizure susceptibility and behavior. Human Molecular Genetics. 2015; 24(5):1457–1468. [PubMed: 25378553]

Golding NL, Staff NP, Spruston N. Dendritic spikes as a mechanism for cooperative long-term potentiation. Nature. 2002; 418(6895):326–331. [PubMed: 12124625]

Gong B, Rhodes KJ, Bekele-Arcuri Z, Trimmer JS. Type I and type II Na(+) channel alpha-subunit polypeptides exhibit distinct spatial and temporal patterning, and association with auxiliary subunits in rat brain. The Journal of Comparative Neurology. 1999; 412(2):342–352. [PubMed: 10441760]

Grunditz A, Holbro N, Tian L, Zuo Y, Oertner TG. Spine neck plasticity controls postsynaptic calcium signals through electrical compartmentalization. The Journal of Neuroscience. 2008; 28(50): 13457–13466. [PubMed: 19074019]

Halasy K, Somogyi P. Distribtuion of GABAergic synapses and their targets in the dentate gyrus of rat: a quantitative immunoelectron microscopic analysis. Journal of Hirnforschung. 1993; 34(3):299–308.

Harnett MT, Makara JK, Spruston N, Kath WL, Magee JC. Synaptic amplification by dendritic spines enhances input cooperativity. Nature. 2012; 491(7425):599–602. [PubMed: 23103868]

He Y, Zorumski CF, Mennerick S. Contribution of presynaptic Na(+) channel inactivation to paired-pulse synaptic depression in cultured hippocampal neurons. Journal of Neurophysiology. 2002; 87(2):925–936. [PubMed: 11826057]

He B, Soderlund DM. Human embryonic kidney (HEK293) cells express endogenous voltage-gated sodium currents and Na_V 1.7 sodium channels. Neuroscience Letters. 2010; 469(2):268–272. [PubMed: 20006571]

Hemmings HC Jr, Girault JA, Nairn AC, Bertuzzi G, Greengard P. Distribution of protein phosphatase inhibitor-1 in brain and peripheral tissues of various species: comparison with DARPP-32. Journal of Neurochemistry. 1992; 59(3):1053–1061. [PubMed: 1353788]

Herold KF, Hemmings HC Jr. Sodium channels as targets for volatile anesthetics. Frontiers in Pharmacology. 2012; 3:50. [PubMed: 22479247]

Hodgkin AL, Huxley AF. Currents carried by sodium and potassium ions through the membrane of the giant axon of Loligo. The Journal of Physiology. 1952; 116(4):449–472. [PubMed: 14946713]

Hsu SM, Raine L, Fanger H. Use of avidin-biotin-peroxidase complex (ABC) in immunoperoxidase techniques: a comparison between ABC and unlabeled antibody (PAP) procedures. The Journal of Histochemistry and Cytochemistry. 1981; 29(4):577–580. [PubMed: 6166661]

Hu W, Tian C, Li T, Yang M, Hou H, Shu Y. Distinct contributions of Na(v)1.6 and Na(v)1.2 in action potential initiation and backpropagation. Nature Neuroscience. 2009; 12(8):996–1002. [PubMed: 19633666]

Jensen HS, Grunnet M, Bastlund JF. Therapeutic potential of Na(v)1.1 activators. Trends in Pharmacological Sciences. 2014; 35(3):113–118. [PubMed: 24439681]

Kim Y, Hsu CL, Cembrowski MS, Mensh BD, Spruston N. Dendritic sodium spikes are required for long-term potentiation at distal synapses on hippocampal pyramidal neurons. Elife. 2015; 4:06414.

Köhrmann M, Haubensak W, Hemraj I, Kaether C, Lessmann VJ, Kiebler MA. Fast, convenient, and effective method to transiently transfect primary hippocampal neurons. Journal of Neuroscience Research. 1999; 58(6):831–835. [PubMed: 10583914]

Kosaka T, Kosaka K, Tateishi K, Hamaoka Y, Yanaihara N, Wu YJ, Hama K. GABAergic neurons containing CCK-8-like and/or VIP-like immunoreactivities in the rat hippocampus and dentate gyrus. Journal of Comparative Neurology. 1985; 239(4):420–430. [PubMed: 2413092]

Kosaka T, Wu JY, Benoit R. GABAergic neurons containing somatostatin-like immunoreactivity in the rat hippocampus and dentate gyrus. Experimental Brain Research. 1988; 71(2):388–398. [PubMed: 3169171]

Lai HC, Jan LY. The distribution and targeting of neuronal voltage-gated ion channels. Nature Reviews Neuroscience. 2006; 7(7):548–562. [PubMed: 16791144]

Larkum ME, Zhu JJ. Signaling of layer 1 and whisker-evoked Ca2+ and Na+ action potentials in distal and terminal dendrites of rat neocortical pyramidal neurons in vitro and in vivo. The Journal of Neuroscience. 2002; 22(16):6991–7005. [PubMed: 12177197]

Liao Y, Deprez L, Maljevic S, Pitsch J, Claes L, Hristova D, Lerche H. Molecular correlates of age-dependent seizures in an inherited neonatal-infantile epilepsy. Brain. 2010; 133(Pt 5):1403–1414. [PubMed: 20371507]

Liu C, Tan FC, Xiao ZC, Dawe GS. Amyloid precursor protein enhances Na_v 1.6 sodium channel cell surface expression. The Journal of Biological Chemistry. 2015; 290(19):12048–12057. [PubMed: 25767117]

Lorincz A, Nusser Z. Cell-type-dependent molecular composition of the axon initial segment. The Journal of Neuroscience. 2008; 28(53):14329–14340. [PubMed: 19118165]

Lorincz A, Nusser Z. Molecular identity of dendritic voltage-gated sodium channels. Science. 2010; 328(5980):906–909. [PubMed: 20466935]

Magee JC, Johnston D. A synaptically controlled, associative signal for Hebbian plasticity in hippocampal neurons. Science. 1997; 275(5297):209–213. [PubMed: 8985013]

Malenka RC. The long-term potential of LTP. Nature Reviews Neuroscience. 2003; 4(11):923–926. [PubMed: 14595403]

Malenka RC, Nicoll RA. NMDA-receptor-dependent synaptic plasticity:multiple forms and mechanisms. Trends in Neurosciences. 1993; 16(12):521–527. [PubMed: 7509523]

Mantegazza M, Curia G, Biagini G, Ragsdale DS, Avoli M. Voltage-gated sodium channels as therapeutic targets in epilepsy and other neurological disorders. Lancet Neurology. 2010; 9(4): 413–424. [PubMed: 20298965]

Martina M, Vida I, Jona SP. Distal initiation and active propagation of action potentials in interneuron dendrites. Science. 2000; 287(5451):295–300. [PubMed: 10634782]

Meeks JP, Mennerick S. Selective effects of potassium elevations on glutamate signaling and action potential conduction in hippocampus. The Journal of Neuroscience. 2004; 24(1):197–206. [PubMed: 14715952]

Megías M, Emri Z, Freund TF, Gulyás AI. Total number and distribution of inhibitory and excitatory synapses on hippocampal CA1 pyramidal cells. Neuroscience. 2001; 102(3):527–540. [PubMed: 11226691]

Mickus T, Jung HY, Spruston N. Slow sodium channel inactivation in CA1 pyramidal cells. Annals of the New York Academy of Sciences. 1999; 868:97–101. [PubMed: 10414288]

Milner TA, Waters EM, Robinson DC, Pierce JP. Degenerating processes identified by electron microscopic immunocytochemical methods. Methods in Molecular Biology. 2011; 793:23–59. [PubMed: 21913092]

Ogiwara I, Miyamoto H, Morita N, Atapour N, Mazaki E, Inoue I, Yamakawa K. Na_V 1.1 localizes to axons of parvalbumin-positive inhibitory interneurons: a circuit basis for epileptic seizures in mice carrying an Scn1a gene mutation. The Journal of Neuroscience. 2007; 27(22):5903–5914. [PubMed: 17537961]

Osorio N, Alcaraz G, Padilla F, Couraud F, Delmas P, Crest M. Differential targeting and functional specialization of sodium channels in cultured cerebellar granule cells. Journal of Physiology. 2005; 569(Pt 3):801–816. [PubMed: 16210352]

Peters, A., Palay, SL., Webster, HD. The fine structure of the nervous system. 3. New York: Oxford UP; 1991.

Pierce JP, Kurucz OS, Milner TA. Morphometry of a peptidergic transmitter system: dynorphin B-like immunoreactivity in the rat hippocampal mossy fiber pathway before and after seizures. Hippocampus. 1999; 9(3):255–276. [PubMed: 10401641]

Sampo B, Tricaud N, Leveque C, Seagar M, Couraud F, Dargent B. Direct interaction between synpatotagmin and the intracellular loop I-II of neuronal voltage-sensitive sodium channels. Proceedings of the National Academy of Sciences of the United States of America. 2000; 97(7): 3666–3671. [PubMed: 10737807]

Sanders SJ, Murtha MT, Gupta AR, Murdoch JD, Raubeson MJ, Willsey AJ, State MW. De novo mutations revealed by whole-exome sequencing are strongly associated with autism. Nature. 2012; 485(7397):237–241. [PubMed: 22495306]

Schmunk G, Gargus JJ. Channelopathy pathogenesis in autism spectrum disorders. Frontiers in Genetics. 2013; 4:222. [PubMed: 24204377]

Sjöstrom PJ, Nelson SB. Spike timing, calcium signals and synaptic plasticity. Current Opinion in Neurobiology. 2002; 12(3):305–314. [PubMed: 12049938]

Soriano E, Frotscher M. A GABAergic axo-axonic cell in the fascia dentate controls the main excitatory hippocampal pathway. Brain Research. 1989; 503(1):170–174. [PubMed: 2611653]

Spencer JL, Waters EM, Milner TA, McEwen BS. Estrous cycle regulates activation of hippocampal Akt, LIM kinase, and neurotrophin receptors in C57BL/6 mice. Neuroscience. 2008; 155(4):1106–1119. [PubMed: 18601981]

Stuart G, Spruston N, Sakmann B, Häusser M. Action potential initiation and backpropagation in neurons of the mammalian CNS. Trends in Neurosciences. 1997; 20(3):125–131. [PubMed: 9061867]

Svoboda K, Helmchen F, Denk W, Tank DW. Spread of dendritic excitation in layer 2/3 pyramidal neurons in rat barrel cortex in vivo. Nature Neuroscience. 1999; 2(1):65–73. [PubMed: 10195182]

Swanson, LW. Brain maps: Structure of the rat brain. 3. Massachusetts: Academic Press; 2003.

Tavassoli T, Kolevzon A, Wang AT, Curchack-Lichtin J, Halpern D, Schwartz L, Buxbaum JD. De novo SCN2A splice site mutation in a boy with Autism spectrum disorder. BMC Medical Genetics. 2014; 15:35. [PubMed: 24650168]

Tian C, Wang K, Ke W, Guo H, Shu Y. Molecular identity of axonal sodium channels in human cortical pyramidal cells. Frontiers in Cellular Neuroscience. 2014; 8:297. [PubMed: 25294986]

Tippens AL, Lee A. Caldendrin, a neuron-specific modulator of Cav/1.2 (L-type) Ca2+ channels. The Journal of Biological Chemistry. 2007; 282(11):8464–8473. [PubMed: 17224447]

Tønnesen J, Nägerl UV. Dendritic spines as tunable regulators of synaptic signals. Frontiers in Psychiatry. 2016; 7:101. [PubMed: 27340393]

Trimmer JS, Rhodes KJ. Localization of voltage-gated ion channels in mammalian brain. Annual Review of Physiology. 2004; 66:477–519.

Tsai MS, Lee ML, Chang CY, Fan HH, Yu IS, Chen YT, Lin SW. Functional and structural deficits of the dentate gyrus network coincide with emerging spontaneous seizures in an Scn1a mutant Dravet Syndrome model during development. Neurobiology of Disease. 2015; 77:35–48. [PubMed: 25725421]

Tsay D, Yuste R. Role of dendritic spines in action potential backpropagation: a numerical simulation study. Journal of Neurophysiology. 2002; 88(5):2834–2845. [PubMed: 12424316]

van Groen T, Wyss JM. Extrinsic projections from area CA1 of the rat hippocampus: olfactory, cortical, subcortical, and bilateral hippocampal formation projections. Journal of Comparative Neurology. 1990; 302(3):515–528. [PubMed: 1702115]

van Wart A, Trimmer JS, Matthews G. Polarized distribution of ion channels within microdomains of the axon initial segment. The Journal of Comparative Neurology. 2007; 500(2):339–352. [PubMed: 17111377]

Waxman SG. Mechanisms of disease: sodium channels and neuroprotection in multiple sclerosis-current status. Nature Clinical Practice Neurology. 2008; 4(3):159–169.

Westenbroek RE, Merrick DK, Catterall WA. Differential subcellular localization of the RI and RII Na^+ channel subtypes in central neurons. Neuron. 1989; 3(6):695–704. [PubMed: 2561976]

Xu J, Kang N, Jiang L, Nedergaard M, Kang J. Activity-dependent long-term potentiation of intrinsic excitability in hippocampal CA1 pyramidal neurons. The Journal of Neuroscience. 2005; 25(7): 1750–1760. [PubMed: 15716411]

Yu FH, Catterall WA. Overview of the voltage-gated sodium channel family. Genome Biology. 2003; 4(3):207. [PubMed: 12620097]

Yu FH, Mantegazza M, Westenbroek RE, Robbins CA, Kalume F, Burton KA, Catterall WA. Reduced sodium current in GABAergic interneurons in a mouse model of severe myoclonic epilepsy in infancy. Nature Neuroscience. 2006; 9(9):1142–1149. [PubMed: 16921370]

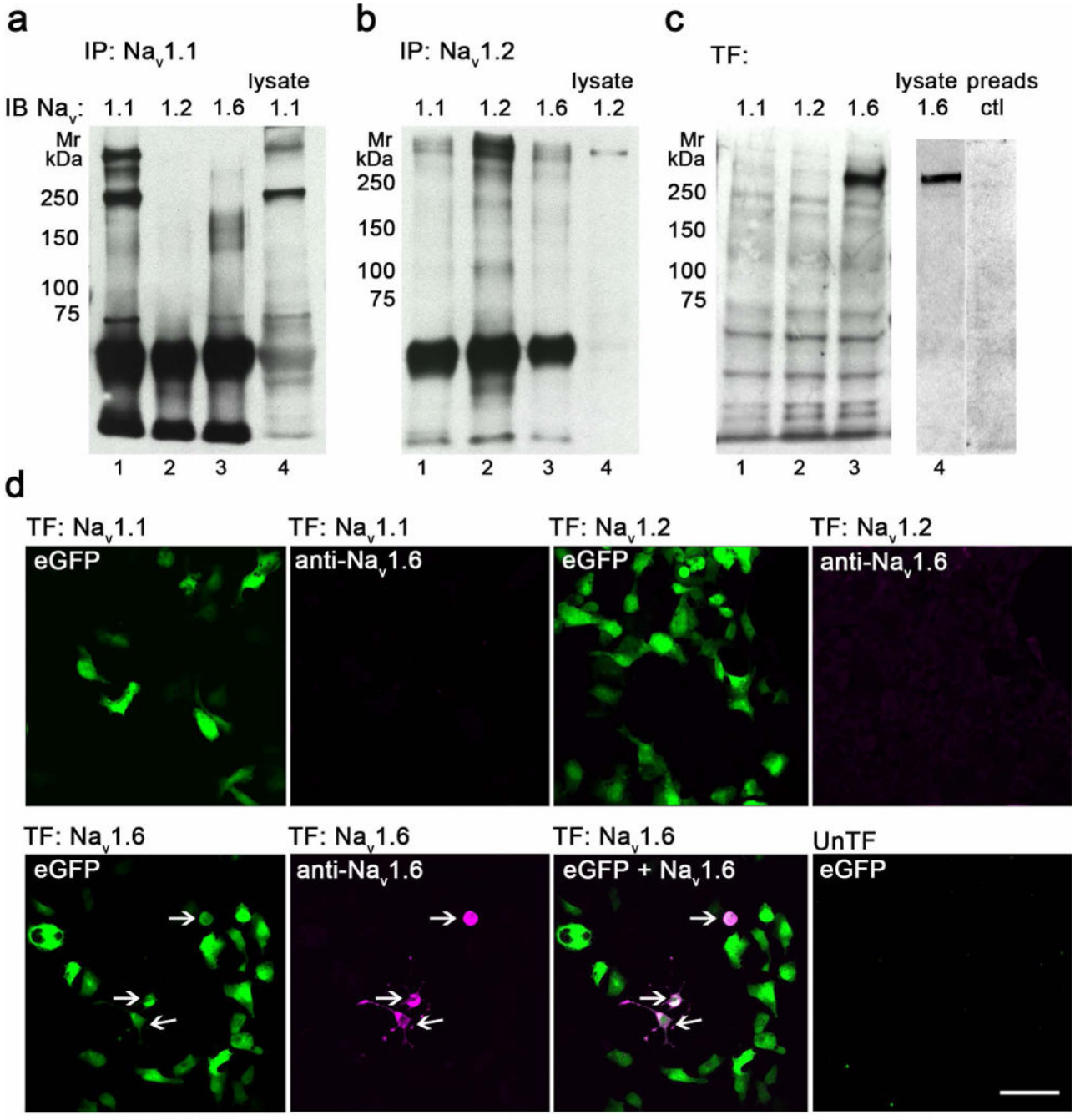

Figure 1.

Validation of anti-Na_v 1.1, anti-Na_v 1.2 and anti-Na_v 1.6 specificities. **A-B.** Na_v 1.1 **(A)** and Na_v 1.2 **(B)** were immunoprecipitated (IP) from rat brain hippocampus lysates and immunoblotted (IB) with anti-Na_v 1.1, anti-Na_v 1.2, and anti-Na_v 1.6 antibodies (lanes 1-4). **C.** HEK293FT cells were transfected (TF) with human Na_v 1.1 (lane 1), rat Na_v 1.2 (lane 2) or mouse Na_v 1.6 (lane 3) and immunoblotted with anti-Na_v 1.6 antibody. Hippocampal lysate (lane 4) and a pre-adsorption peptide (lane 5) were used as a positive and negative control, respectively. The blocking peptide, made up of the same sequences as the Na_v 1.6

antibody, specifically blocks expression of Na_v 1.6 from the hippocampal lysate. **D.** HEK293FT cells were transfected (TF) with eGFP (green fluorescence) and human Na_v 1.1 (top left 2 panels), rat Na_v 1.2 (top, right 2 panels) or mouse Na_v 1.6 (bottom 3 panels), and immunolabeled with anti-Na_v 1.6 with detection using AlexaFluor-568-conjugated secondary antibody (magenta fluorescence). All cells expressing Na_v 1.6 co-expressed eGFP (arrows). Untransfected cells (bottom right) served as a negative control. Mr, relative molecular mass (in kDa). Bar 75 μm. See supplemental figure 1 for red-green images.

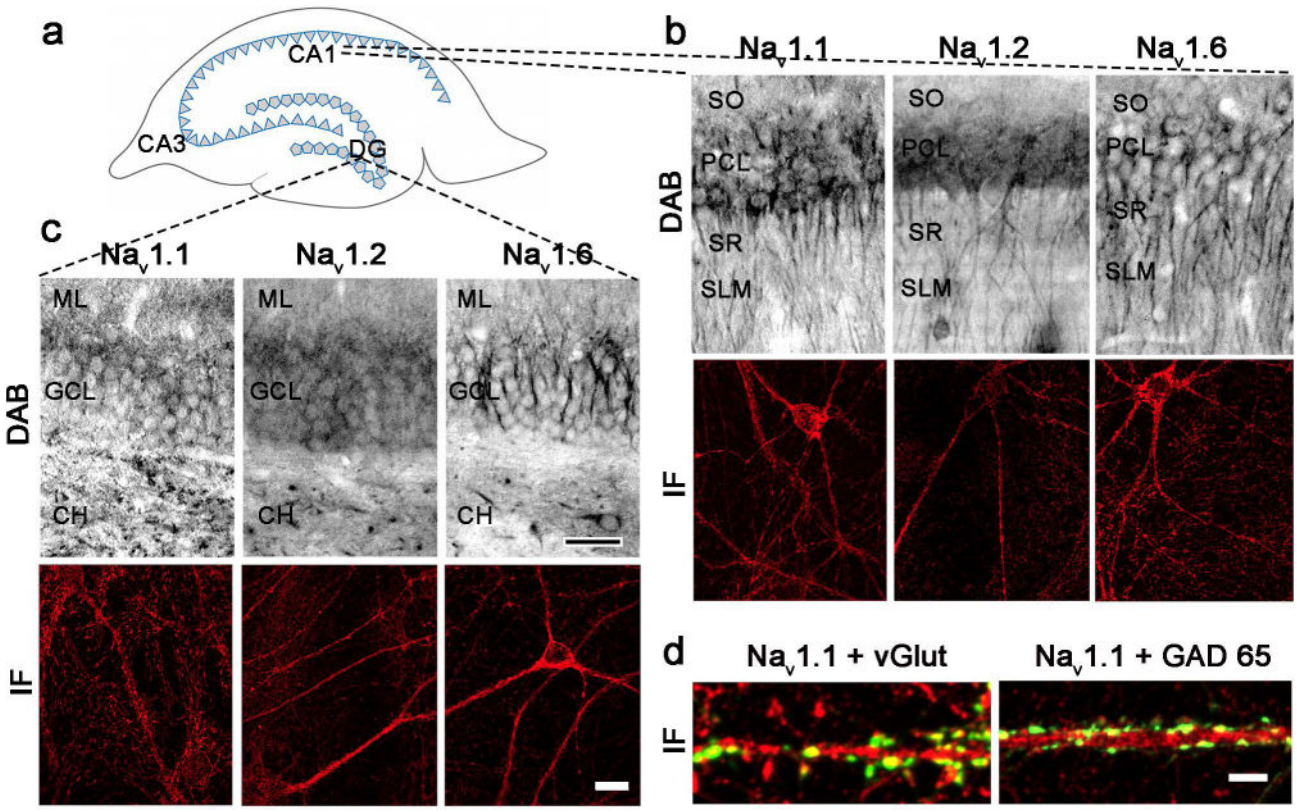

Figure 2.

Na$_v$ subtypes are expressed in soma, dendrites and axons of hippocampal CA1 and DG. **A.** Schematic diagram of CA1, CA3, and dentate gyrus (DG) in rat hippocampus. **B-C**. High magnification light microscopic photomicrographs (top) of Na$_v$ 1.1 (left), Na$_v$ 1.2 (middle), and Na$_v$ 1.6 (right) in rat CA1 **(B)** and DG **(C)**. Na$_v$ labeling is evident in stratum oriens (SO), pyramidal cell layer (PCL), stratum radiatum (SR), and stratum lacunosum-moleculare (SLM) in CA1 **(B, top)** and in molecular layer (ML), granular cell layer (GCL), and central hilus (CH) in DG **(C, top)**. Bar 200 μm. Examples of immunofluorescence localization of Na$_v$ 1.1 (left), Na$_v$ 1.2 (middle), and Na$_v$ 1.6 (right) in rat hippocampal cultures from CA1 (**B**, bottom) and DG (**C**, bottom). Bar 15 μm. **D.** Immunofluorescence images showing double labeling of Na$_v$ 1.1 (magenta) with excitatory axon terminal marker vesicular glutamate transporter (vGlut; green, left) and inhibitory axon terminal marker glutamic acid decarboxylase 65 (GAD 65; green, right). Bar 5 μm. See supplemental figure 2 for red-green images.

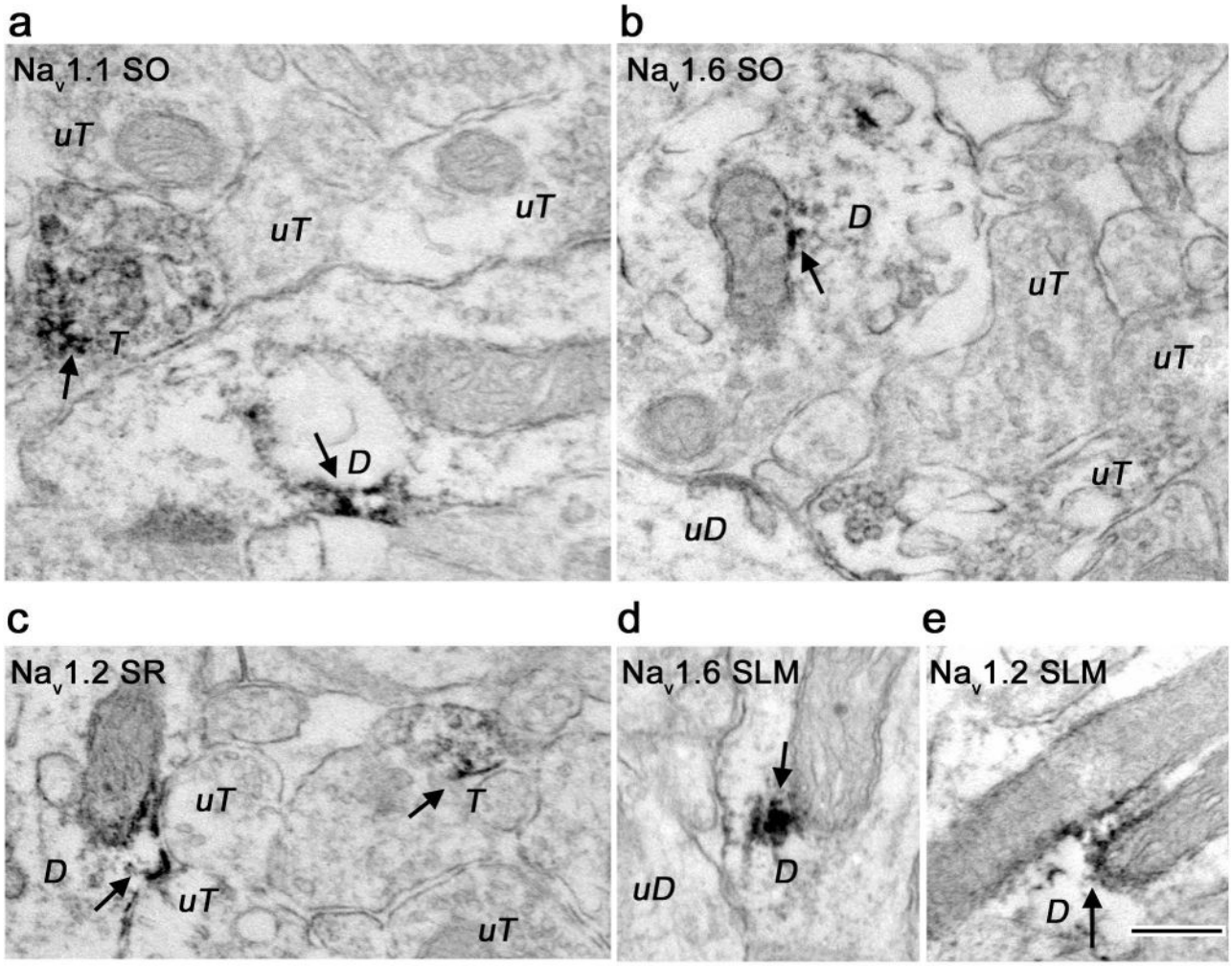

Figure 3.

Electron micrographs showing dendritic localization of Na_v 1.1, Na_v 1.2, and Na_v 1.6 immunoreactivity in hippocampal subregions. **A.** Na_v 1.1 immunoreactivity in CA1 stratum oriens (SO) was present in a dendritic shaft. Adjacent labeled terminal (*T*) and unlabeled terminals (*uT*) are also shown. **B, D**. Na_v 1.6 immunoreactivity in discrete patches within a cross-section (**B**) or longitudinal section (**D**) of a dendrite in subregions SO and stratum lacunosum-moleculare (SLM). Unlabeled dendrites (*uD*) and terminals (*uT*) are shown for comparison. **C, E.** CA1 stratum radiatum (SR) and SLM Na_v 1.2 immunoreactivity was frequently associated with mitochondrial endomembranes (*D*). Unlabeled terminals (*uT*) are found nearby (**C**). Immunoreactivity is shown with arrows. Bar 250 nm.

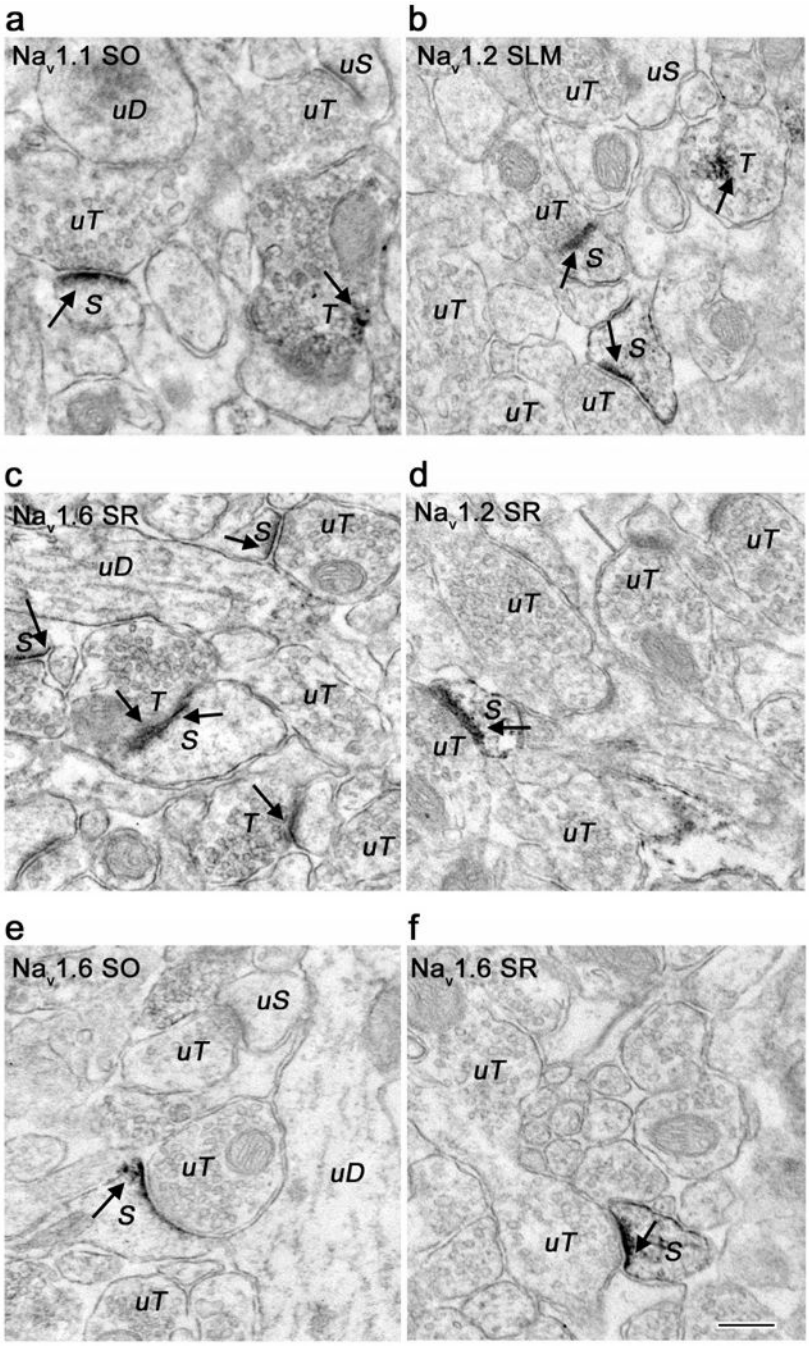

Figure 4.

Electron micrographs showing localization of Na_v 1.1, Na_v 1.2, and Na_v 1.6 immunoreactivity in dendritic spines. **A.** Na_v 1.1 immunoreactive dendritic spine (*S*) forms a synapse with an unlabeled terminal (*uT*) in CA1 stratum oriens (SO). Discrete labeling was seen predominantly in the spine head. Nearby unlabeled dendrite (*uD*) and terminal (*uT*) as well as a labeled terminal (*T*) are shown for comparison. **B, D.** Na_v 1.2 immunoreactivity in CA1 stratum-lacunosum-moleculare (SLM) and stratum radiatum (SR) in labeled spine heads and spine necks (*S*) forming synapses with unlabeled terminals (*uT*). Two labeled

branching spines are seen in panel **B**. Nearby labeled (*T*) and unlabeled terminals (*uT*) are shown. **C, E, F.** Na_v 1.6 immunoreactivity in dendritic spines in CA1 SO, SR, and SLM. Multiple labeled spines (*S*) are seen in panel **C** forming synapses with labeled (*T*) and unlabeled (*uT*) terminals. Immunoreactivity shown with arrows. Bar 250 nm.

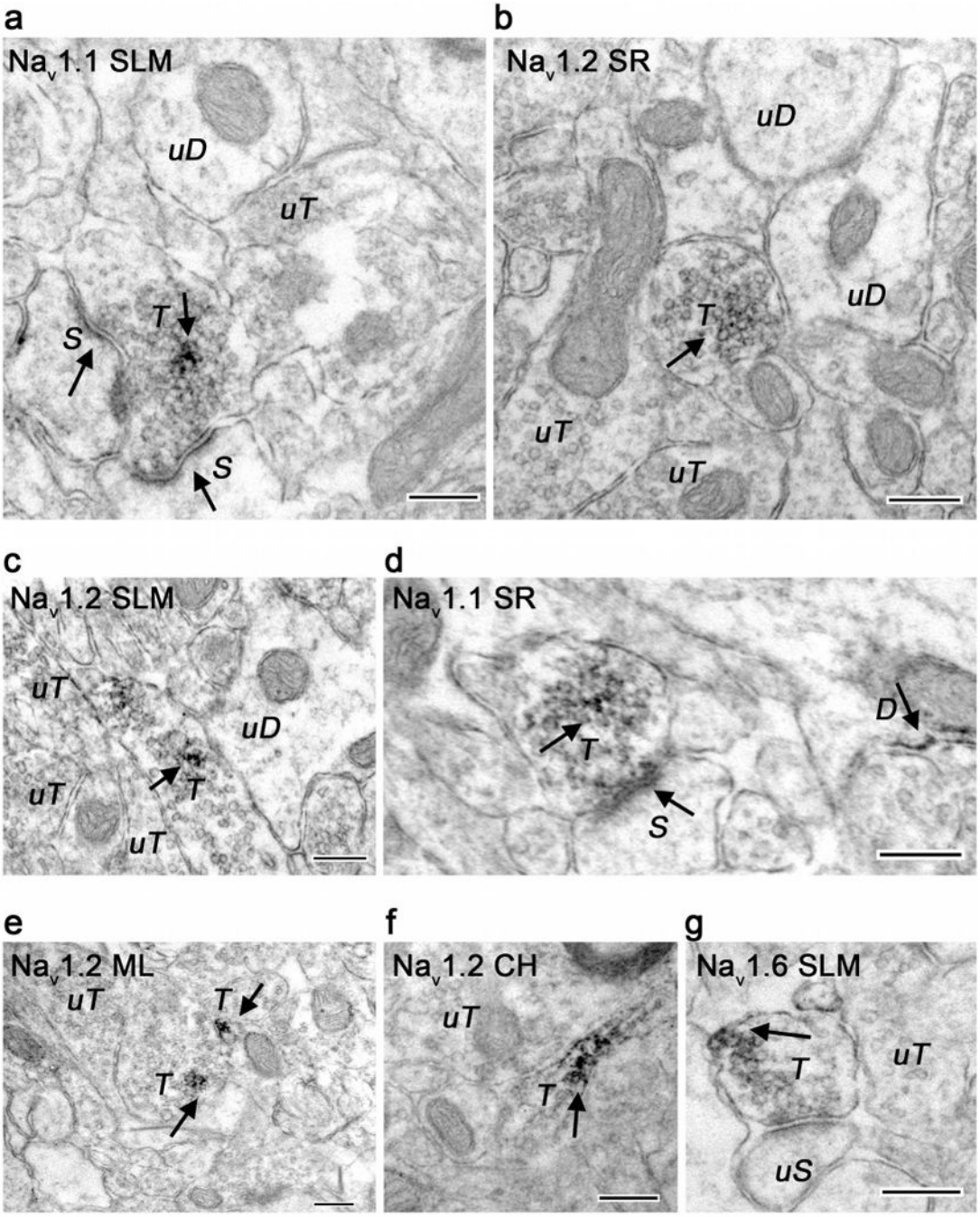

Figure 5.

Electron micrographs showing axonal localization of Na_v 1.1, Na_v 1.2, and Na_v 1.6 immunoreactivity in hippocampal subregions. **A, D.** Na_v 1.1 labeled axon terminals (*T*) synapse with labeled dendritic spines (*S*). Labeled (*D*) and unlabeled dendrites (*uD*) and terminals (*uT*) are seen nearby. **B, C, E, F.** Most Na_v 1.2 immunoreactive axons in CA1 stratum radiatum (SR), stratum lacunosum-moleculare (SLM) and DG molecular layer (ML) and central hilum (CH) do not form synapses. **G.** Na_v 1.6 immunoreactivity was found in

CA1 (SLM) associated with an unlabeled spine (*uS*). Immunoreactivity shown with arrows. Bar 250 nm.

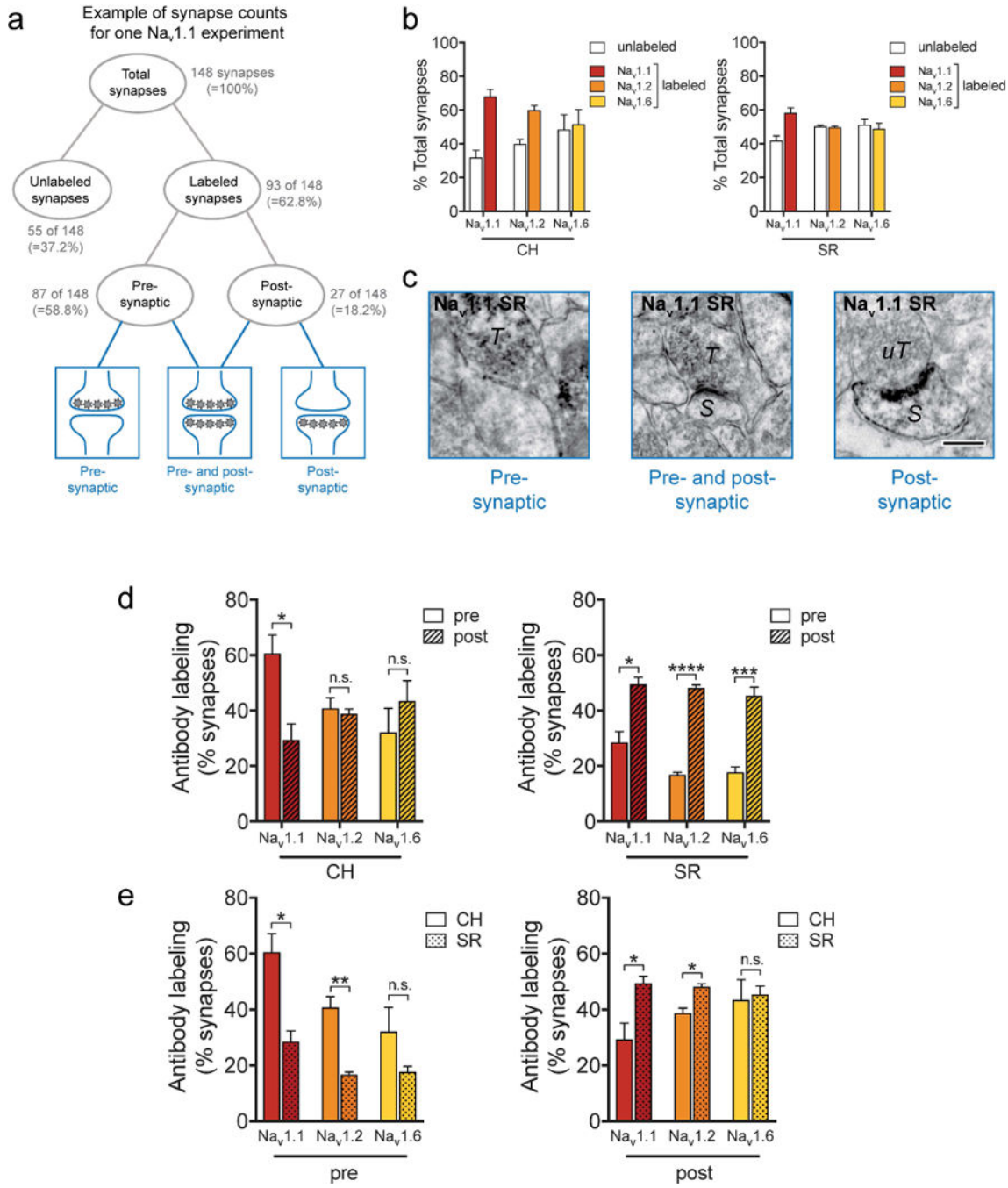

Figure 6.

Synapses in the DG central hilus (CH) express more Na_V 1.1 in axon terminals and synapses in the CA1 stratum radiatum (SR) express more Na_V 1.1 and Na_V 1.2 in dendrites and spines. **A**. Schematic diagram showing example of data quantification. All labeled and unlabeled synapses were identified (**A**, top; **B**). Labeled synapses were further categorized as pre- (**C**, left), post- (**C**, right), or pre-and postsynaptic (**C**, middle) labeling (**A**, bottom; **C**). Bar graphs show labeling in pre- or post-synaptic compartments divided by total number of synapses **(B, D, E)**; unlabeled synapses made up 30-50% of total synapses (**B**). **C**. Na_V 1.1

immunoreactive axon terminal (*T*) next to an unlabeled postsynaptic compartment in the SR (left). A Na_v 1.1 immunoreactive axon terminal (*T*) synapses with labeled spine (*S*) in the SR (middle). A Na_v 1.2 immunoreactive spine (*S*) synapses with an unlabeled axon terminal (*uT*) in the SR (right). Bar 250 nm. **D.** Quantitative analysis shows that Na_v 1.1 immunoreactivity is significantly more presynaptic in the CH (left), whereas all Na_v 1 subtypes are significantly more postsynaptic in the SR (right). Data were analyzed from 15 micrographs obtained from three rats per experimental group; n = 352 to 398 profiles in CH and 654 to 698 profiles in SR**. E.** Quantitative analysis showing axon terminals in the CH express more Na_v 1.1 and Na_v 1.2 labeling compared to axon terminals in the SR, and that dendrites and spines in the CH express less Na_v 1.1 and Na_v 1.2 labeling compared to dendrites and spines in the SR. Data were analyzed from 15 micrographs obtained from three rats per experimental group; n = 110 to 167 profiles in presynaptic compartments and 98 to 352 profiles in postsynaptic compartments. * $p<0.05$, ** $p<0.01$, *** $p<0.001$, **** $p<0.0001$, n.s.-not significant.

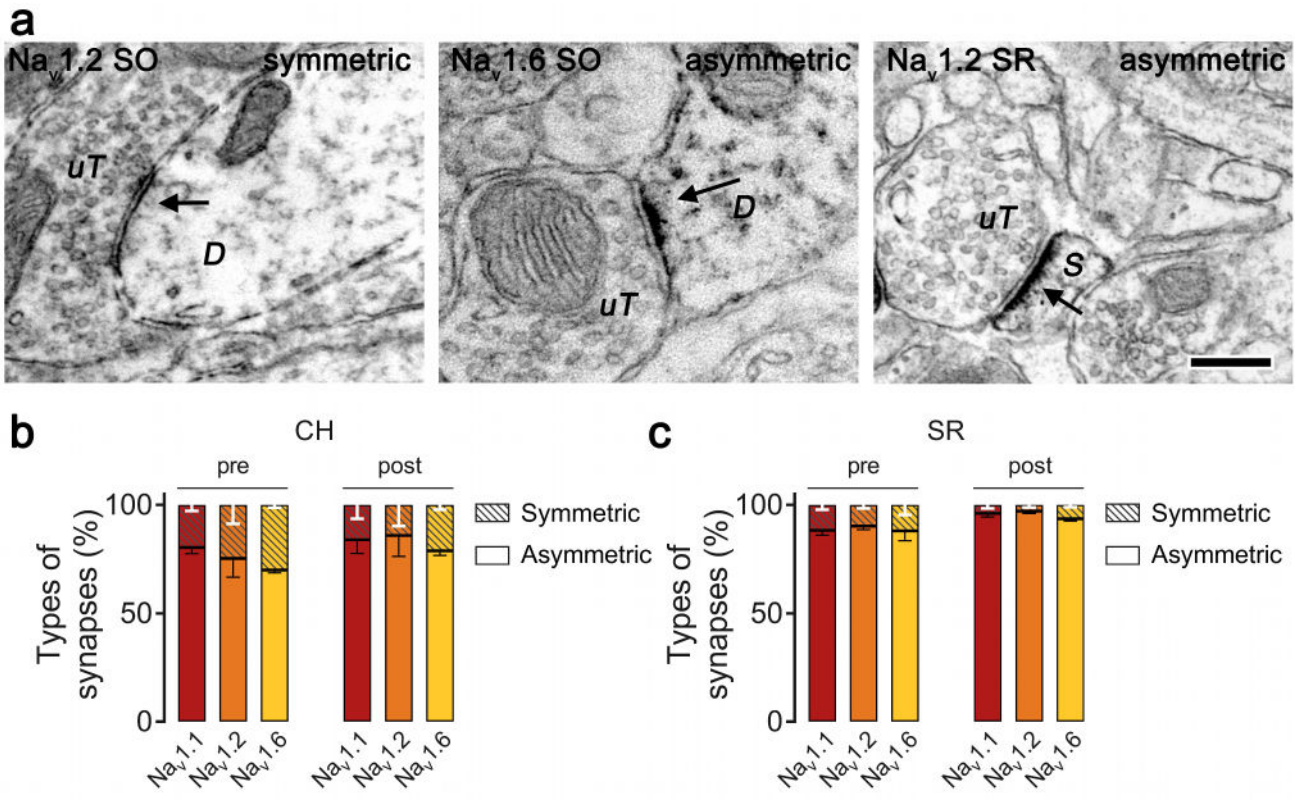

Figure 7.

Na$_v$ immunoreactivity is predominantly associated with asymmetric synapses in the stratum radiatum (SR) and central hilus (CH) subregions. **A.** A Na$_v$ 1.2 unlabeled terminal (*uT*) is seen making a symmetric synapse with a labeled dendrite (*D*; left) and a labeled spine (*S*; right). A Na$_v$ 1.6 unlabeled terminal is seen making an asymmetric synapse with a labeled dendrite (*D*; middle). Bar 250 nm. **B, C.** Quantitative analysis showing pre- and post-synaptic structures containing Na$_v$ immunoreactivity is largely associated with asymmetric synapses in the SR **(B)** and CH **(C).** Data were analyzed from 15 micrographs obtained from three rats per experimental group; n = 265 to 316 synapses in CH and 424 to 540 synapses in SR.

Table 1

Overview of antibody characteristics

Antigen	Immunogen	Manufacturer	Concentration
Na_v 1.1	Synthetic peptide, amino acid sequence (C)TASEHSREPSAAGRLSD from rat Na_v 1.1, intracellular loop between domains I and II; residues 465-481	Alomone; rabbit polyclonal antibody; ASC_001; RRID:AB_2040003	1:400 (ICC) 0.6 μg/ml (IP/IB)
Na_v 1.2	Synthetic peptide, amino acid sequence (C)ASAESRDFSGAGGIGVFSE from rat Na_v 1.2, intracellular loop between domains I and II; residues 467-485	Alomone; rabbit polyclonal antibody; ASC_002; RRID:AB_2040005	1:200 (ICC) 0.8 μg/ml (IP/IB)
Na_v 1.6	Synthetic peptide, amino acid sequence (C)IANHTGVDIHRNGDFQKNG from rat Na_v 1.6, intracellular loop between domains II and III; residues 1042-1061	Alomone; rabbit polyclonal antibody; ASC_009; RRID:AB_2040202	1:800 (ICC) 0.8 μg/ml (IP/IB)

Abbreviations: IB, immunoblotting; ICC, immunocytochemistry; IP, immunoprecipitation.